UCSF
UC San Francisco Previously Published Works

Title
Protective Role of IL-6 in Vascular Remodeling in Schistosoma Pulmonary Hypertension

Permalink
https://escholarship.org/uc/item/7gg7521m

Journal
American Journal of Respiratory Cell and Molecular Biology, 49(6)

ISSN
1044-1549

Authors
Graham, Brian B
Chabon, Jacob
Kumar, Rahul
et al.

Publication Date
2013-12-01

DOI
10.1165/rcmb.2012-0532oc

Peer reviewed

eScholarship.org Powered by the California Digital Library
University of California

Protective Role of IL-6 in Vascular Remodeling in *Schistosoma* Pulmonary Hypertension

Brian B. Graham[1,3], Jacob Chabon[1], Rahul Kumar[1], Ewa Kolosionek[3,4], Liya Gebreab[1], Elias Debella[1], Michael Edwards[1], Katrina Diener[1], Ted Shade[1], Gao Bifeng[1], Angela Bandeira[5], Ghazwan Butrous[3,6], Kenneth Jones[2], Mark Geraci[1,3], and Rubin M. Tuder[1,3]

[1]Program in Translational Lung Research, Division of Pulmonary Sciences and Critical Care Medicine, and [2]Division of Biochemistry and Molecular Genetics, Department of Medicine, University of Colorado School of Medicine, University of Colorado Denver, Aurora, Colorado; [3]Pulmonary Vascular Research Institute, and [4]Department of Medical Biochemistry and Microbiology, Biomedical Center, University of Uppsala, Uppsala, Sweden; [5]Division of Cardiology, Memorial San José Hospital, Universidade de Pernambuco, Recife, Brazil; and [6]School of Pharmacy, University of Kent, Kent, United Kingdom

Schistosomiasis is one of the most common causes of pulmonary arterial hypertension worldwide, but the pathogenic mechanism by which the host inflammatory response contributes to vascular remodeling is unknown. We sought to identify signaling pathways that play protective or pathogenic roles in experimental *Schistosoma*-induced pulmonary vascular disease via whole-lung transcriptome analysis. Wild-type mice were experimentally exposed to *Schistosoma mansoni* ova by intraperitoneal sensitization followed by tail-vein augmentation, and the phenotype was assessed by right ventricular catheterization and tissue histology, as well as RNA and protein analysis. Whole-lung transcriptome analysis by microarray and RNA sequencing was performed, and RNA sequencing was analyzed according to two bioinformatics methods. Functional testing of the candidate IL-6 pathway was determined using IL-6 knockout mice and the signal transducers and activators of transcription protein–3 (STAT3) inhibitor S3I-201. Wild-type mice exposed to *S. mansoni* demonstrated increased right ventricular systolic pressure and thickness of the pulmonary vascular media. Whole-lung transcriptome analysis determined that the IL-6–STAT3–nuclear factor of activated T cells c2(NFATc2) pathway was up-regulated, as confirmed by PCR and the immunostaining of lung tissue from *S. mansoni*–exposed mice and patients who died of the disease. Mice lacking IL-6 or treated with S3I-201 developed pulmonary hypertension, associated with significant intima remodeling after exposure to *S. mansoni*. Whole-lung transcriptome analysis identified the up-regulation of the IL-6–STAT3–NFATc2 pathway, and IL-6 signaling was found to be protective against *Schistosoma*-induced intimal remodeling.

Keywords: pulmonary hypertension; schistosomiasis; gene expression profiling; IL-6

CLINICAL RELEVANCE

Schistosomiasis is a major cause of pulmonary hypertension worldwide, but has not been significantly studied. The inflammatory nature of this disease may have applicability to other forms of inflammatory pulmonary vascular disease. We performed whole-transcriptome analysis of a mouse model of this disease, identified potentially pathogenic signaling processes, confirmed the results at the protein level in human and mouse tissue, and modulated the pathway in the mouse at two levels. Our results have the potential to guide future treatments of inflammatory pulmonary vascular diseases.

Schistosomiasis is one of the most common causes of World Health Organization (WHO) Group 1 pulmonary arterial hypertension (PAH) worldwide. More than 200 million people in 74 countries are infected with *Schistosoma* spp., and approximately 5–15 million people chronically and recurrently infected with *Schistosoma mansoni* manifest PAH, a progressive and fatal pulmonary vascular disease (1–4). Schistosomiasis-associated PAH shares common pulmonary vascular pathology with other forms of PAH, including remodeling of the vascular media and intima, resulting in vascular obstruction (5). Studies aimed at identifying the pathogenesis of schistosomiasis-associated PAH have revealed key roles of T helper (Th)2-mediated inflammation, which may also participate in other forms of PAH in which inflammation likely contributes to the disease, including idiopathic PAH (IPAH), connective tissue disease–associated PAH (6), and hypoxic pulmonary hypertension (PH) (7).

Mice exposed to *S. mansoni* develop experimental pulmonary hypertension (PH), which recapitulates several key features of the human disease, including increased right ventricular (RV) pressure, pulmonary vascular remodeling, and RV hypertrophy. RV hypertrophy in particular is associated with augmented IL-13 signaling or more prolonged *S. mansoni* infection (8–10). We previously documented that the up-regulation of IL-13 after *S. mansoni* infection may be sufficient for experimental PH (8), which also provides a context for similar data connecting Th2 inflammation with PH observed in mice exposed to inhaled *Aspergillus* (11) and in IL-13–overexpressing mice (12).

To delineate further the potential mechanisms involved in *S. mansoni* PH, we pursued the identification of potentially relevant pathways with whole-genome expression profiling in the relevant mouse model of the disease. We performed whole-transcriptome analysis, using multiple approaches to cross-validate the data and to explore reproducibility with a specific model system, followed by determining the functional role of an identified pathway within the animal model. Guided by these approaches, we found a protective role for IL-6 signaling in endothelial cells in this model of Th2-

(*Received in original form December 28, 2012 and in final form May 28, 2013*)

This work was supported by an Advancing Science through Pfizer–Investigator Research Exchange (B.B.G.), National Institutes of Health grant K08HL105536 (B.B.G.), a Parker B. Francis Fellowship (B.B.G.), National Institutes of Health grant RC1HL100849 (R.M.T.), the Cardiovascular Medical Research and Education Fund (R.M.T.), the Genomics and Biostatistics/Bioinformatics Shared Resources of Colorado's National Institutes of Health/National Cancer Institute Cancer Center Support Grant P30CA046934, and National Institutes of Health/National Center for Advancing Translational Sciences Colorado Clinical and Translational Science Institute grant UL1 TR000154.

Correspondence and requests for reprints should be addressed to Brian B. Graham, M.D., Program in Translational Lung Research, Division of Pulmonary Sciences and Critical Care Medicine, Department of Medicine, University of Colorado School of Medicine, University of Colorado Denver, 12700 East 19th Avenue, Aurora, CO 80045. E-mail: brian.graham@ucdenver.edu

This article has an online supplement, which is accessible from this issue's table of contents at www.atsjournals.org

Am J Respir Cell Mol Biol Vol 49, Iss. 6, pp 951–959, Dec 2013
Copyright © 2013 by the American Thoracic Society
Originally Published in Press as DOI: 10.1165/rcmb.2012-0532OC on July 1, 2013
Internet address: www.atsjournals.org

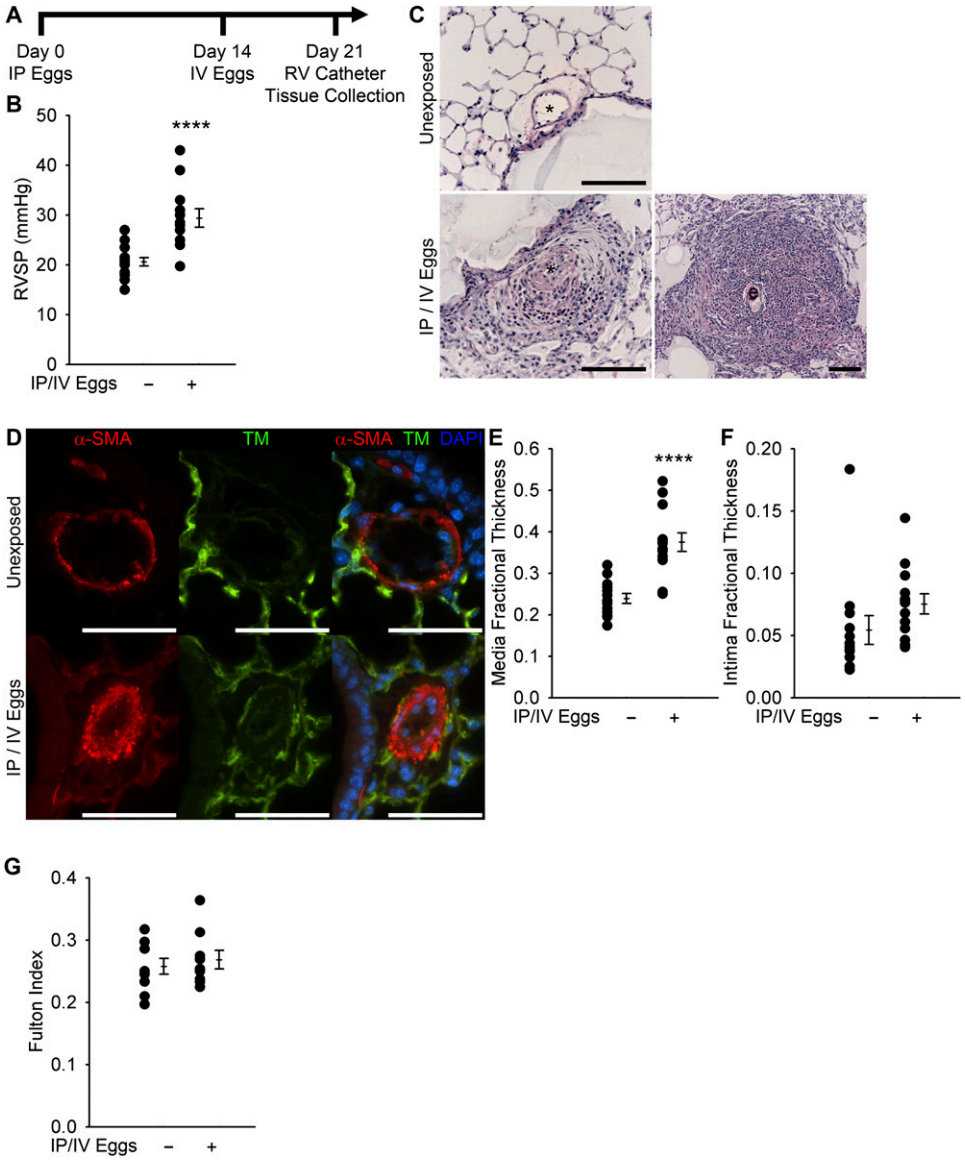

Figure 1. Mice exposed to *Schistosoma mansoni* eggs develop pulmonary hypertension (PH) and vascular remodeling. (*A*) Experimental protocol of intraperitoneal (IP) sensitization and intravenous (IV) augmentation with *S. mansoni* eggs. (*B*) Right ventricular systolic pressure (RVSP; mean ± SE; $n = 12$–14 mice per group; *t* test, ****$P < 0.001$). (*C*) Representative hematoxylin-and-eosin staining of unexposed and IP/IV egg–exposed mouse lungs (*vessel lumen; e, *S. mansoni* egg; *scale bars*, 100 μm). (*D*) Representative immunofluorescence staining for α–smooth muscle actin (α-SMA) and thrombomodulin (TM) demonstrates vascular remodeling (*scale bars*, 50 μm). (*E* and *F*) Quantitative fractional thickness of the pulmonary vascular media and intima in unexposed and IP/IV egg–exposed mice (mean ± SE; $n = 13$ mice per group; *t* test; media, ****$P < 0.001$; intima, $P =$ no significance). (*G*) Fulton index (ratio of right ventricular mass to mass of left ventricle + septum) of unexposed and IP/IV egg–exposed mice (mean ± SE; $n = 9$–10 mice per group; *t* test, $P =$ no significance).

induced PH. This finding underscores the potentially contrasting roles of IL-6 in PH, because IL-6 plays pathogenic roles in other forms of experimental PH. Some of our findings have been previously reported as an abstract (13).

MATERIALS AND METHODS

Mouse Model

Wild-type C57Bl6/J mice and IL-$6^{-/-}$ mice on a C57Bl6/J background (The Jackson Laboratories, Bar Harbor, ME) were used. We relied on a previously reported mouse model of experimental schistosomiasis-induced PH (8), which models the natural history of the parasite infection, notably in relation to the pulmonary vascular disease. Briefly, mice receive 240 purified *S. mansoni* eggs/gram body weight (purified from the livers of infected Swiss-Webster mice, provided by the Biomedical Research Institute, Rockville, MD) injected intraperitoneally, followed 2 weeks later by challenge with 240 *S. mansoni* eggs/gram body weight injected by tail vein. One week after the intravenous challenge, the mice underwent terminal RV catheterization. Formalin-fixed and paraffin-embedded lung tissue was analyzed for vascular remodeling and peri-egg granuloma size, as previously described (8). Frozen lung tissue was analyzed for the number of remaining eggs, as previously described (8). S3I-201 (EMD Millipore, Billerica, MA) was reconstituted in DMSO, diluted in PBS, and administered at 5 mg/kg or the equivalent volume of vehicle alone intraperitoneally, at the time points shown. Additional details regarding the animal experiments and statistical analyses are described in the online supplement. All mice were bred and housed under specific pathogen–free conditions in a facility approved by the American Association for the Accreditation of Laboratory Animal Care. All experimental procedures in rodents were approved by the Animal Care and Use Committees at the University of Colorado Denver.

Sources of Human Tissue

Tissue from patients who died of schistosomiasis-associated PAH was used for immunostaining experiments. This tissue had been previously collected during autopsies at the Memorial San José Hospital (Universidade de Pernambuco, Recife, Pernambuco, Brazil), and was formalin-fixed and paraffin-embedded. The analysis of autopsy tissue was interpreted as non–human subject research by the Colorado Institutional Review Board and the review board in Pernambuco.

Messenger RNA Measurement by Microarray and RNA Sequencing

Messenger RNA (mRNA) was retrieved from *S. mansoni*–exposed and unexposed wild-type mice. The mRNA expression levels were quantified using an Affymetrix Mouse Gene ST1.0 microarray (Affymetrix Inc., Santa Clara, CA). The mRNA expression levels were also quantified using an Illumina HiSeq 2000 RNA sequencing (RNA-seq) system (Illumina Inc., San Diego, CA). The reads were single-directional, and 100 bases in length (for seven samples, two control samples and one

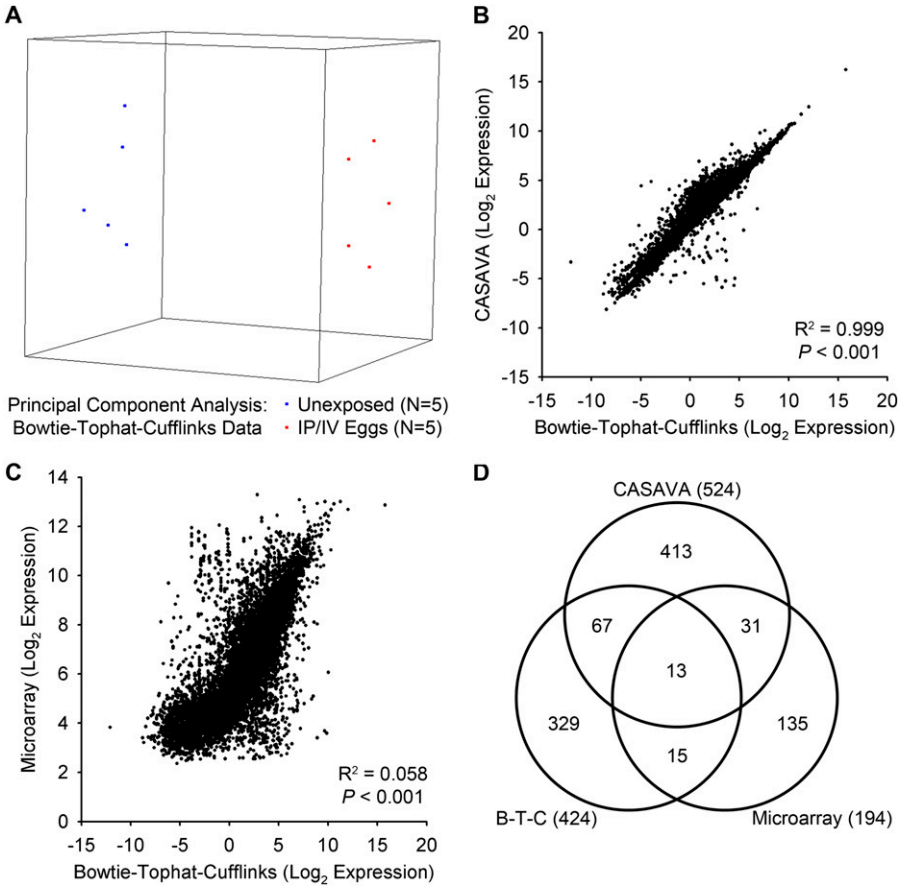

Figure 2. Whole-transcriptome principal components analysis (PCA) and comparison of RNA sequencing (RNA-seq) to microarray results. (*A*) Multidimensional PCA using RNA-seq data, as analyzed by Bowtie–TopHat–Cufflinks, separates groups according to exposure status ($n = 5$ per group). (*B* and *C*) Analyses of the same RNA from a single uninfected mouse were used to compare gene expression levels according to (*B*) Bowtie–TopHat–Cufflinks versus CASAVA and (*C*) Bowtie–TopHat–Cufflinks versus microarray. (*D*) Venn diagram of genes identified as significantly modulated after *S. mansoni* infection, using $n = 10$ (five IP/IV egg–exposed, five unexposed) for the RNA-seq data, and $n = 6$ (three IP/IV egg–exposed, and three unexposed) for the microarray data. B-T-C, Bowtie–TopHat–Cufflinks.

intraperitoneal/intravenous [IP/IV] egg–exposed sample underwent 50 base-length, single-stranded reads). The RNA-seq reads were mapped to the mouse National Center for Biotechnology Information Build 37/Mus musculus version 9 (mm9) genome, using two bioinformatics platforms: the proprietary Illumina system CASAVA (version 1.7), and the open-source system Bowtie–TopHat–Cufflinks, using the web-based interface Galaxy (http://main.g2.bx.psu.edu). CASAVA version 1.7 uses the ELAND version 2 alignment algorithm (14). Bowtie uses the Burrows–Wheeler transform for alignment, TopHat identifies splice junctions, and Cufflinks assembles and quantifies levels of transcription (15–17). The parameters used for Bowtie–TopHat–Cufflinks are listed in Table E1 in the online supplement. The data discussed in this publication have been deposited in NCBI's Gene Expression Omnibus and are accessible through GEO Series accession number GSE49116. Additional details of RNA retrieval, analysis, and bioinformatics approaches are described in the online supplement.

RNA Analysis by RT-PCR and Protein Analysis by Immunostaining and Immunoblotting

The RNA quantification by RT-PCR of mouse lung tissue and protein analysis by the immunostaining and immunoblotting of mouse and human lung tissue was used to confirm the whole-transcriptome analysis. Primers, immunostaining reagents, and immunoblotting reagents are listed in Table E2.

RESULTS

Mice Exposed to *S. mansoni* Eggs Demonstrate Increased Right Ventricular Pressure and Vascular Remodeling

Similar to our previous findings (8), mice intraperitoneally sensitized and intravenously exposed to *S. mansoni* eggs developed a significant increase in RV systolic pressure (RVSP; $P < 0.001$; Figures 1A and 1B). The observed histopathology included vascular remodeling and peri-egg granulomas (Figure 1C). The quantification of vascular remodeling by immunostaining for α–smooth muscle actin (media) and thrombomodulin (intima) revealed significant thickening of the pulmonary arterial vascular media and little change in the intima (Figures 1D–1F). No significant right ventricular hypertrophy, as measured by the Fulton index, or significant alterations in systemic hemodynamics (Figure 1G and Table E3) were evident.

Whole-Transcriptome Analyses by Microarray and RNA-Seq Identify Modulated Genes

We sought to identify potentially relevant signaling pathways that link the inflammatory and immune responses to *S. mansoni* exposure with the PH phenotype. We used two platforms for whole-lung transcriptome measurement, namely, microarray and RNA-seq. Six samples (three unexposed, and three IP/IV egg–exposed) were analyzed, using both platforms. In addition, four more wild-type samples (two unexposed, and two IP/IV egg–exposed) were analyzed by RNA-seq alone. The number of RNA-seq reads for each sample was between 1.6×10^7 and 3.0×10^7. All RNA-seq data were subsequently analyzed, using two bioinformatics pipelines, namely, CASAVA and Bowtie–TopHat–Cufflinks. Because of the differing types of methodologies, each may strive to analyze its own unique set of transcripts. For this analysis, we found 14,248 genes that were mutually analyzed by all methods. Thus we narrowed the focus of this study to this set of genes. Multidimensional principal component analysis (PCA) was used to confirm the separation of the sample transcriptomes into two discrete groups according to exposure status. The PCA plots generated from Bowtie–TopHat–Cufflinks for all 10 samples (Figure 2A) and the PCA plots for the CASAVA and microarray results (Figures E1A and E1B) showed a similar clustering of normal

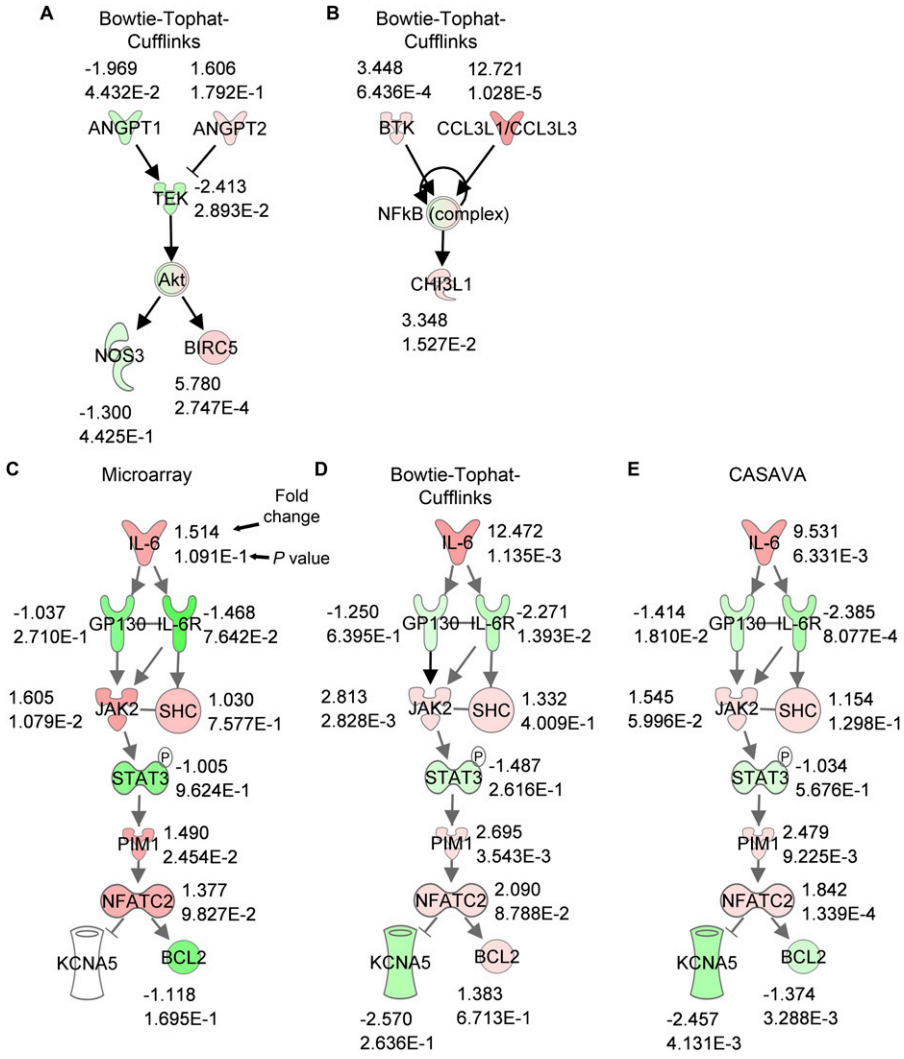

Figure 3. The IL-6–signal transducers and activators of transcription protein–3 (STAT3)–nuclear factor of activated T cells c2 (NFATc2) pathway is identified as up-regulated by whole-lung transcriptome analysis after *S. mansoni* egg exposure in mice. (*A*) Modulation of the angiopoetin–Tie2–survivin pathway after *S. mansoni* exposure by Bowtie–TopHat–Cufflinks (ANGPT1, angiopoietin 1; ANGPT2, angiopoietin 2; TEK, tyrosine kinase that contains immunoglobulin-like loops and epidermal-growth-factor-similar domains 2 (Tie2); BIRC5, survivin). (*B*) Modulation of the NF-κB–chitinase-3–like–1 (Chi3l1) pathway after *S. mansoni* exposure by Bowtie–TopHat–Cufflinks (CCL3L1/CCL3L3 = macrophage inflammatory protein 1a (MIP1a)). *Red*, up-regulated; *green*, down-regulated; the numbers adjacent to each gene indicate fold change and the significance of the change according to *P* value. Modulation of the IL-6–STAT3–NFATc2 pathway after *S. mansoni* exposure by (*C*) microarray, (*D*) Bowtie–TopHat–Cufflinks, and (*E*) CASAVA. Alternative transcriptome analyses of the angiopoetin–Tie2–survivin and NF-κB–Chi3l1 pathways are presented in Figures E6 and E9, respectively.

versus infected gene expression patterns. A discovery plot showing the distribution of *P* values comparing gene expression levels between unexposed and egg-exposed samples for the three approaches is depicted in Figure E1C.

Comparing the results between microarray and RNA-seq analyses for a single uninfected sample demonstrated close correlation between Bowtie–TopHat–Cufflinks and CASAVA ($R^2 = 0.999$; Figure 2B). In contrast, the correlation between microarray and RNA-seq was lower, particularly for low expression genes where RNA-seq demonstrated a wider dynamic range than microarray, as revealed by the "hockey stick" appearance of the comparison plots ($R^2 = 0.058$; Figure 2C). These trends in correlation were present for all unexposed and IP/IV egg–exposed samples (data not shown).

The genes with the greatest differential expression, as identified by each analytical technique, are compared in a Venn diagram (Figure 2D). Differential gene expressions from Bowtie–TopHat–Cufflinks data were analyzed using the algorithm Cuffdiff and the Student *t* test. The results are compared in Figure E2, and Cuffdiff-generated results were used thereafter. Overall, relatively little overlap was evident between the three analysis methods, with only 13 differentially expressed genes identified by all three methods. The overlap of identified genes was not significantly altered by considering only higher or lower expression value genes (Figures E3A and E3B).

A sensitivity analysis was performed with reduced numbers of RNA-seq reads from one RNA-seq sample, as analyzed by Bowtie–TopHat–Cufflinks, to identify how many reads were required to obtain reasonable correlation with the complete dataset. Even at 1.0×10^6 RNA-seq reads, 15,470 genes were identified (79.8% of those identified in the complete dataset), and 85.4% of the expression levels were within twofold of the expression levels from the complete dataset (Figures E4A–E4F and Table E4).

Top Modulated Genes Are in Immunologic and Metabolic Pathways

Thirteen genes were identified as significantly modulated according to all three methods of analysis. These genes are listed in Table E5, with the fold-change and statistical significance determined by all three methods. Up-regulated genes included metabolic (β glucuronidase) and the immune pathway (integrin β2 and tumor necrosis factor receptor superfamily, member 9), consistent with the metabolic and immune activity in the lungs of *S. mansoni* egg–exposed mice. One hundred and twenty-six genes were identified as significantly altered in expression by at least two analysis methods, and a gene ontology analysis of this subset was performed using ingenuity pathways analysis to identify the top altered signaling networks and cellular functions (Tables E6 and E7). Again, most of the networks and functions

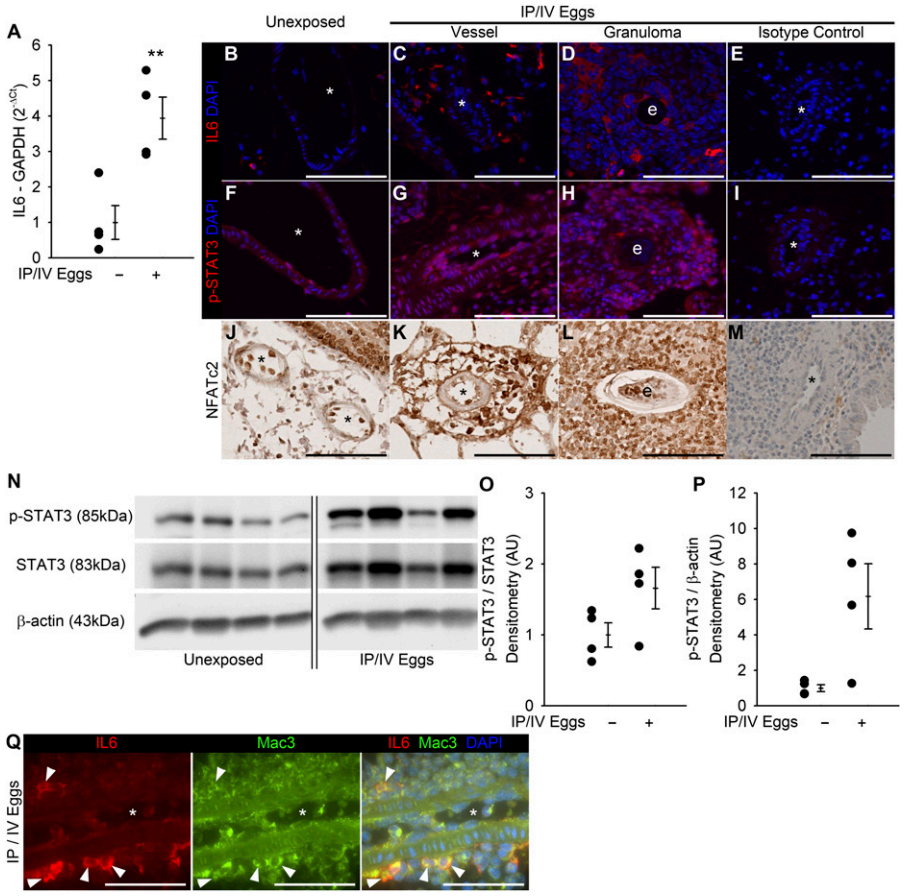

Figure 4. Confirmation of the activation of the IL-6–STAT3–nuclear factor of activated T cells c2 (NFATc2) pathway in mouse tissue. (*A*) RT-PCR for IL-6 relative to glyceraldehyde 3–phosphate dehydrogenase (GAPDH; mean ± SE; $n = 4$ mice per group; *t* test, $^{**}P < 0.01$). (*B–E*) Immunostaining for IL-6 in unexposed and IP/IV egg–exposed mouse tissue, with isotype control (*vessel lumen; e, egg; *scale bars*, 100 μm). (*F–I*) Immunostaining for phospho-S727-STAT3 in unexposed and IP/IV egg–exposed mouse tissue, with isotype control (*vessel lumen; e, egg; *scale bars*, 100 μm). (*J–M*) Immunostaining for NFATc2 in unexposed and IP/IV egg–exposed mouse tissue, with isotype control (*vessel lumen; e, egg; *scale bars*, 100 μm). (*N–P*) Immunoblot of whole-lung lysates from unexposed and IP/IV egg-exposed mice, probed for phospho-S727-STAT3 (p-STAT3), total STAT3, and β-actin loading control, with ratios of densitometry for phospho-STAT3 to total STAT3 and phospho-STAT3 to β-actin (AU, arbitrary units; normalized to mean of unexposed mice = 1; mean ± SE; $n = 4$ mice per group; *t* test, $P =$ no significance for both; Western blot images are cropped: intact Western blots are shown in Figure E14). (*Q*) Colocalization by immunostaining for IL-6 and Mac3, a marker of macrophage lysosomes; additional images are presented in Figure E11 (*arrowheads* show colocalized stain; *vessel lumen; *scale bars*, 50 μm). DAPI, 4′,6-diamidino-2-phenylindole.

involved metabolism or the immune response. In particular, the most modulated network centered around NF-κB, urokinase plasminogen activator, and transforming growth factor–β (TGF-β; Figure E5).

The whole-lung transcriptome analysis encompasses both the peri-egg granulomas and vascular disease compartments, which coincide with the pathological alterations seen in *Schistosoma*-induced PH. Moreover, the parasite-induced inflammatory process and pulmonary vascular remodeling appear to be mechanistically linked. To pursue pathways involved in the interactions between inflammation and pulmonary vascular disease, we selected three significantly modulated candidate pathways, which could be pathogenic for the development of PH on the basis of biologic plausibility, for confirmatory protein and mechanistic analyses.

RNA levels in the angiopoetin–tyrosine kinase that contains immunoglobulin-like loops and epidermal-growth-factor-similar domains 2 (Tie2/Tek)–survivin pathway appeared to be significantly altered by *S. mansoni* egg exposure (Figures 3A and E6), with egg-exposed mice demonstrating a down-regulation of angiopoietin 1 (Ang1) and a trend toward the up-regulation of Ang2,-both of which would exert the effect of suppressing their receptor Tie2 (18). Whole-lung lysate immunoblots demonstrated trends toward up-regulation in the protein levels of Ang2 and the Tie2 target survivin (Figures E7A–E7D). An increase was also evident in adventitial lung survivin in exposed mice according to immunostaining, but with little change in the media (which was already present in unexposed mice) or peri-egg granulomas (Figures E7E–E7H). These findings differed somewhat from those obtained via the immunostaining of human lung tissue, collected during autopsies from individuals in Brazil who died of schistosomiasis-associated PAH, compared with normal lungs from failed donors, which demonstrated an increase of survivin in the vascular media (Figure E8).

Chitinase-3–like–1 (Chi3l1) is a Th2-related, chitinase-like gene. Chi3l1 was highly up-regulated in IP/IV egg–exposed mice (Figures 3B and E9). Chi3l1 may be dependent on NF-κB signaling (19), which, as already noted, appeared to be modulated after *S. mansoni* egg exposure. However, immunoblots of whole-lung lysates showed similar expression levels of phospho–NF-κB and total NF-κB levels after *S. mansoni* egg exposure, while a trend toward more Chi3l1 expression was evident (Figures E10A–E10F). Immunostaining lung tissue for Chi3l1 also revealed more prominent airway epithelial staining in *S. mansoni*–exposed mice compared with unexposed mice, with staining at the edges of peri-egg granulomas, but little vascular staining (Figures E10G–E10J).

Finally, the IL-6–signal transducers and activators of transcription protein–3 (STAT3)–nuclear factor of activated T cells c2 (NFATc2) pathway was highly up-regulated in IP/IV egg–exposed mice, as assessed by all three RNA quantification methods (Figures 4A–4C). Based on previous studies demonstrating STAT3 activation and NFATc2 up-regulation in other human and mouse models of (PH) (20, 21), and based on demonstrations that IL-6 overexpression is sufficient to cause spontaneous PH in the mouse (22), we selected this pathway for further study.

Confirmation of IL-6–STAT3–NFATc2 Activation in Mouse and Human Tissue

Real-time PCR for IL-6 confirmed that IL-6 mRNA levels were increased in *S. mansoni*–exposed mice, compared with unexposed mice (Figure 4A). Immunostaining demonstrated increased IL-6 in the peri-egg granulomas and adventitial infiltrates in *S. mansoni*–exposed mice, increased phospho-STAT3

in pulmonary vascular endothelial cells as well as in the adventitia and peri-egg granulomas, and increased NFATc2 in the adventitia and peri-egg granulomas in egg-exposed mice (Figures 4B–4M). Immunoblots of whole-lung lysates showed a trend toward increased phospho-S727-STAT3 (Figures 4N–4P). Costaining with the macrophage lysosome marker Mac3 (23) demonstrated that adventitial and granuloma IL-6 colocalized with macrophages (Figure 4Q; additional images and isotype controls are presented in Figure E11).

Human lung tissue immunostaining demonstrated an increased intima and adventitia distribution of IL-6 in individuals who died of schistosomiasis-associated PAH (Figures 5A–5C), consistent with reports of increased serum IL-6 in individuals infected with *S. mansoni* (24). Furthermore, we observed evidence of increased phospho-S727-STAT3 and NFATc2 activity in the media of remodeled vessels, compared with control human lungs (Figures 5D–5I).

IL-6 Exerts Opposing Effects on Intima and Media Remodeling in *S. mansoni*–Induced PH

Based on our observations of increased IL-6–STAT3–NFATc2 pathway activity after *S. mansoni* egg exposure, we sought to determine the role of IL-6 by challenging IL-$6^{-/-}$ mice with an IP sensitization and intravenous augmentation of *S. mansoni* eggs. We found that IL-$6^{-/-}$ mice developed increased RVSP after exposure to *S. mansoni*, at a level comparable to IL-$6^{+/+}$ mice (Figure 6A; results of one-way ANOVA are presented in the figures, and results of two-way ANOVA are presented in Table E8). A quantitative analysis of vascular remodeling revealed that IL-$6^{-/-}$ mice exposed to *S. mansoni* developed a significant increase in intima thickness, with relative protection from the increased media thickness compared with wild-type mice (Figures 6B–6D). Furthermore, after IP/IV egg exposure, the IL-$6^{-/-}$ mice developed RV hypertrophy, as measured by the Fulton index (Figure 6E). No significant difference was evident in the volume of peri-egg granulomas or clearance of eggs from the lungs between IL-$6^{+/+}$ and IL-$6^{-/-}$ mice (Figures 6F and 6G). Immunostaining for phospho-STAT3 and NFATc2 showed some persistent activity despite the absence of IL-6, whereas the immunoblotting of whole-lung lysates showed no significant difference in phospho-STAT3 relative to either total STAT3 or β-actin in IL-$6^{-/-}$ mice (Figure E12).

We also targeted STAT3 activation using the small molecule inhibitor S3I-201, at an effectively preventive dose in a model of systemic hypertension (25). Similar to the IL-$6^{-/-}$ mice, we observed a persistent increase in RVSP and RV hypertrophy despite this treatment, with increased remodeling of the intima compared with mice receiving vehicle alone (Figures 7A–7F; results of one-way ANOVA are presented in the figures, and results of two-way ANOVA are presented in Table E9). However, S3I-201–treated mice did develop media remodeling after

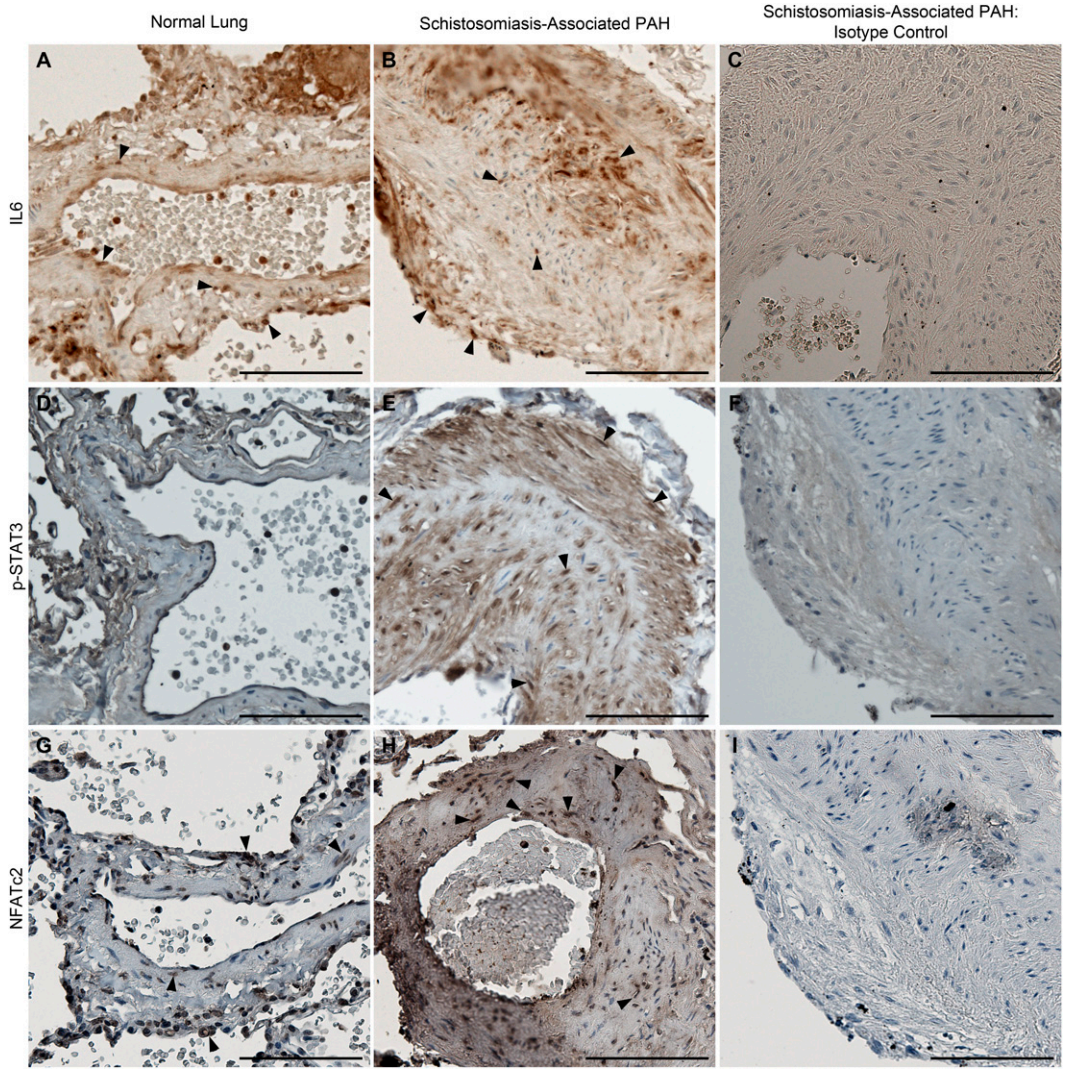

Figure 5. Confirmation of IL-6–STAT3–nuclear factor of activated T cells c2 (NFATc2) pathway activation in human tissue obtained during autopsies from individuals who died of scistosomiasis-associated pulmonary arterial hypertension (PAH), compared with normal human lung tissue (from a failed donor). (*A–C*) Immunostaining for IL-6 in lung tissue from normal control and schistosomiasis-associated PAH, and a specimen stained with isotype control antibody (*arrowheads* show representative positive-stained cells; *scale bars*, 100 μm). (*D–F*) Immunostaining for phospho–serine 727–STAT3 in lung tissue from normal control and schistosomiasis-associated PAH, and a specimen stained with isotype control antibody (*arrowheads* indicate representative positive-stained cells; *scale bars*, 100 μm). (*G–I*) Immunostaining for NFATc2 in lung tissue from normal control and schistosomiasis-associated PAH, and a specimen stained with isotype control antibody (*arrowheads* indicate representative positive-stained cells; *scale bars*, 100 μm).

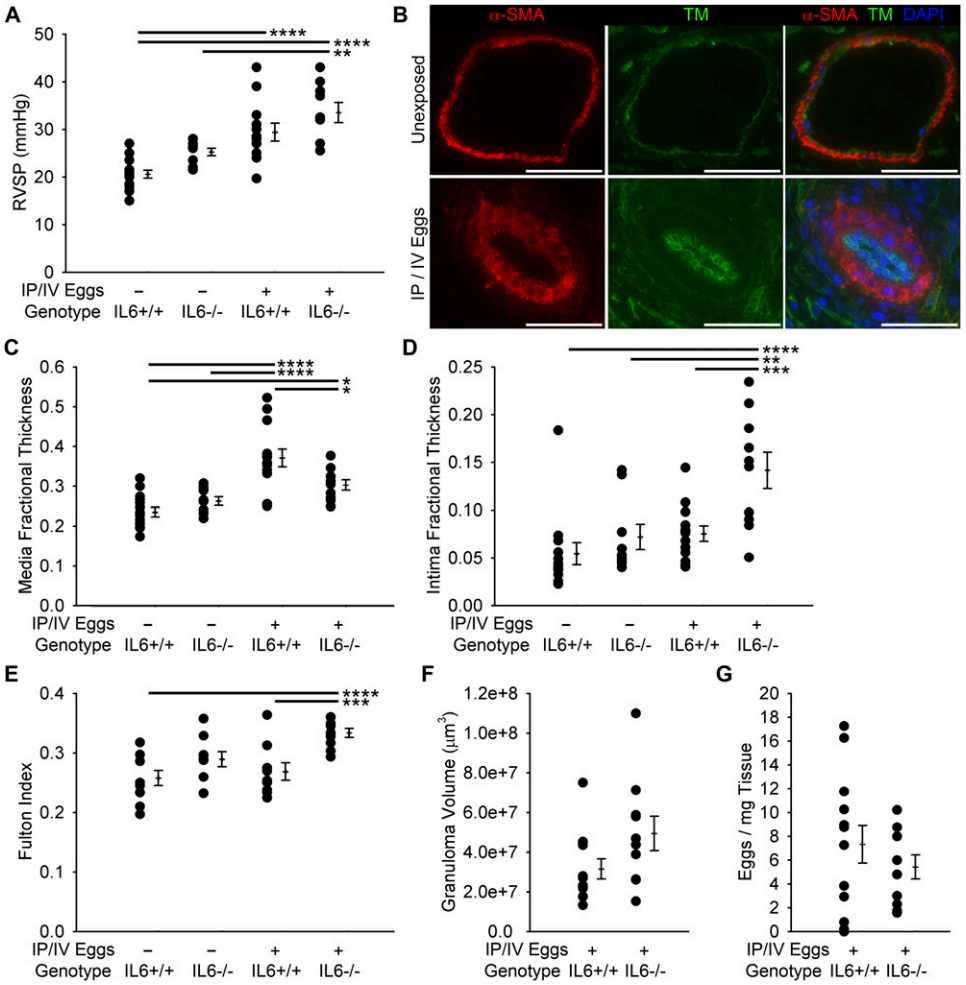

Figure 6. IL-$6^{-/-}$ mice exposed to IP/IV *S. mansoni* eggs develop PH, intima remodeling, and right ventgricular (RV) hypertrophy. (*A*) RVSP in IL-$6^{+/+}$ and IL-$6^{-/-}$ mice unexposed and exposed to *S. mansoni* eggs (mean ± SE; $n = 9$–14 mice per group; ANOVA, $P < 0.001$; *post hoc* Tukey test, $^{**}P < 0.01$, $^{****}P < 0.001$). (*B*) Representative immunofluorescence staining for α-SMA and TM to demonstrate vascular remodeling (*scale bars*, 50 μm). (*C* and *D*) Quantitative fractional thickness of the pulmonary vascular media and intima in unexposed and IP/IV egg–exposed IL-$6^{+/+}$ and IL-$6^{-/-}$ mice (mean ± SE; $n = 9$–13 mice per group; ANOVA, $P < 0.001$ for both; *post hoc* Tukey test, $^{*}P < 0.05$, $^{**}P < 0.01$, $^{***}P < 0.005$, and $^{****}P < 0.001$). (*E*) Fulton index (RV/(left ventricle + septum)) of unexposed and IP/IV egg–exposed IL-$6^{+/+}$ and IL-$6^{-/-}$ mice (mean ± SE; $n = 9$–10 mice per group; ANOVA, $P < 0.001$; *post hoc* Tukey test, $^{***}P < 0.005$ and $^{****}P < 0.001$). (*F*) Peri-egg granuloma volume in IL-$6^{+/+}$ and IL-$6^{-/-}$ *S. mansoni* IP/IV egg–exposed mice (mean ± SE; $n = 10$–12 mice per group; *t* test, $P =$ no significance). (*G*) Egg counts after 4% potassium hydroxide (KOH) digest in IL-$6^{+/+}$ and IL-$6^{-/-}$ IP/IV egg–exposed mice (mean ± SE; $n = 10$–13 mice per group; *t* test, $P =$ no significance). Note that the wild-type data in *A*, *C*, *D*, and *E* are the same as the wild-type data in Figures 1B and 1E–1G, respectively.

egg exposure, in contrast to the IL-$6^{-/-}$ mice. No significant effects on peri-egg granuloma volume or egg clearance with this treatment were evident (Figures 7G and 7H). Immunostaining revealed less vascular phospho-STAT3 and NFATc2 in S3I-201–treated mice, although the quantity of phospho-STAT3 in whole-lung lysates was not significantly altered by this treatment (Figure E13).

DISCUSSION

Little is known about the pathogenic mechanism by which the host immune response contributes to pulmonary vascular disease due to of schistosomiasis, one of the most common causes of WHO Group 1 PAH worldwide. We previously observed that the up-regulation of IL-13 signaling worsened the vascular phenotype, whereas the inhibition of IL-13 signaling alone was inadequate to suppress vascular remodeling completely after *S. mansoni* infection (8). We therefore sought to identify relevant signaling pathways modulating pulmonary vascular disease, using whole-transcriptome analysis. The samples we used for whole-genome analysis represented typical control and infected specimens. Some experimental variation is evident between specific animals (8) (further findings will be presented by Graham and colleagues, to be published), but this was unlikely to alter the results of our studies.

We found little mutual overlap in the quantified transcriptome generated by microarray and two RNA-seq approaches, particularly in regard to the list of genes identified as significantly modulated. However, the discrepancy we observed is comparable to that in previous whole-transcriptome analysis studies. For example, in an analysis of gene expression comparing human lung cancer and noncancer samples, Beane and colleagues (26) reported that of 86 genes found to be differentially expressed by RNA-seq analysis, only 20 (23%) were also differentially expressed by microarray analysis (compared with our observed 30.4% overlap with either of our RNA-seq methods). We also observed a larger dynamic range with RNA-seq than with microarray analysis.

Considerable debate remains regarding the optimum RNA-seq analytical algorithms to measure biologically relevant transcriptome regulation (27). CASAVA (using the ELAND version 2 algorithm) and TopHat (using the Burrows-Wheeler transform) use significantly different approaches in mapping reads to a reference genome. ELAND version 2 creates a table of short reads (length of 32) and identifies matches between these reads and the reference genome, a relatively fast but memory-intensive strategy (14). In contrast, the Burrows-Wheeler transform first permutes the order of the reads to optimize matching, and then identifies matches, a relatively slow but less memory-intensive approach (17). We found that the CASAVA and TopHat–Bowtie–Cufflinks algorithms gave relatively similar but nonidentical results when analyzing the same data. To reduce false-positive results in downstream analyses, we only analyzed genes that were significantly modulated in two or more platforms or pipelines.

A significant limitation of our whole-lung transcriptome approach involved the inclusion of multiple tissue compartments contributing to the mRNA analyzed. Specifically, the compartments analyzed in aggregate included normal lung tissue (parenchyma, airways, and vasculature), along with peri-egg granulomas and remodeled vessels

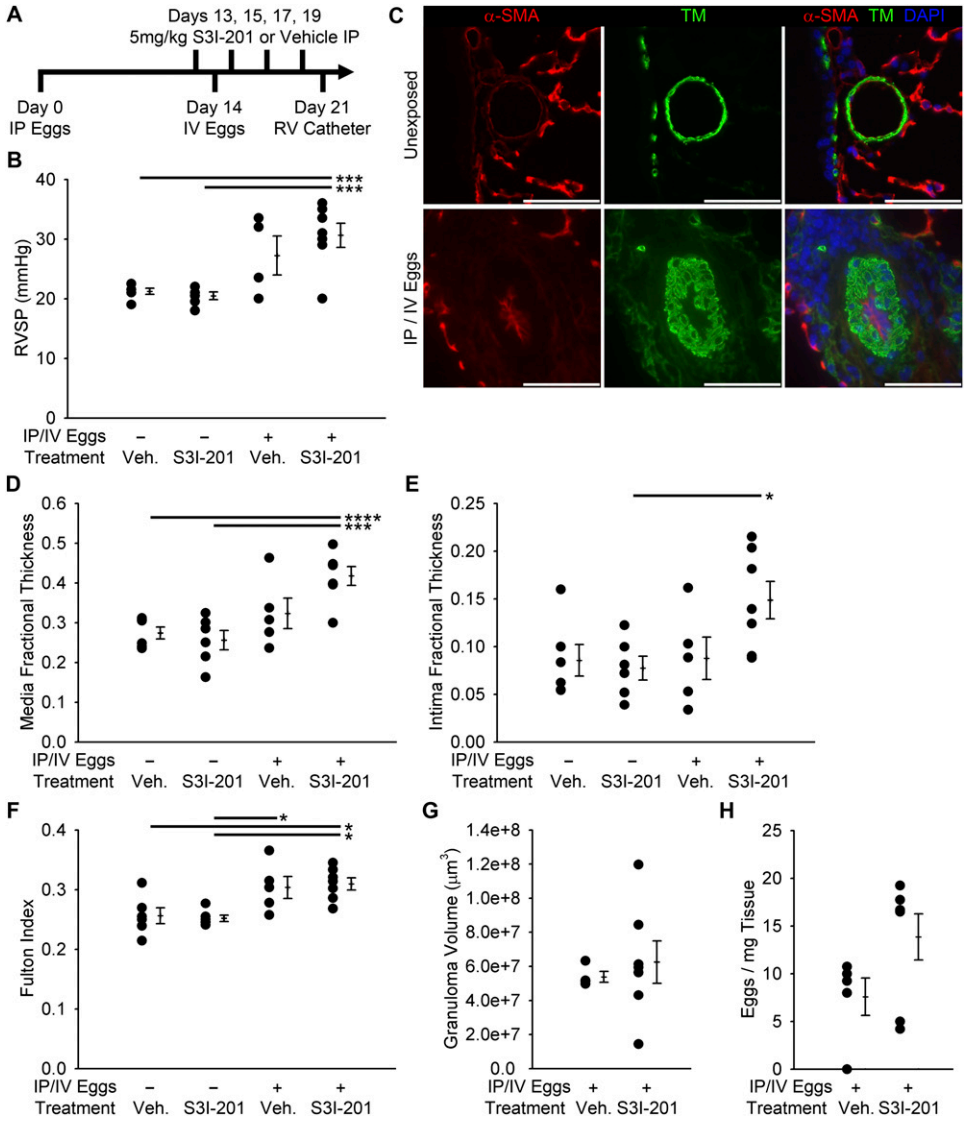

Figure 7. Mice treated with the STAT3 inhibitor S3I-201 develop PH, intima remodeling, and RV hypertrophy after *S. mansoni* egg exposure. (*A*) Experimental protocol of IP/IV *S. mansoni* egg exposure with S3I-201 or vehicle treatment. (*B*) RVSP in vehicle-treated (Veh.) and S3I-201–treated mice, unexposed and exposed to *S. mansoni* eggs (mean ± SE; $n = 4$–7 mice per group; ANOVA, $P < 0.001$; *post hoc* Tukey test, $^{***}P < 0.005$). (*C*) Representative immunofluorescence staining for α-SMA and TM to demonstrate vascular remodeling (*scale bars*, 50 μm). (*D* and *E*) Quantitative fractional thickness of the pulmonary vascular media and intima in S3I-201–treated unexposed and IP/IV egg–exposed mice (mean ± SE; $n = 5$–7 mice per group; ANOVA, $P < 0.001$ for media and $P = 0.029$ for intima; *post hoc* Tukey test, $^{*}P < 0.05$, $^{***}P < 0.005$, and $^{****}P < 0.001$). (*F*) Fulton index of unexposed and IP/IV egg–exposed vehicle-treated and S3I-201–treated mice (mean ± SE; $n = 5$–7 mice per group; ANOVA, $P = 0.003$; *post hoc* Tukey test, $^{*}P < 0.05$). (*G*) Peri-egg granuloma volume in IP/IV egg–exposed vehicle and S3I-201–treated mice (mean ± SE; $n = 4$–7 mice per group; *t* test, $P =$ NS). (*H*) Egg counts after 4% KOH digest in IP/IV egg–exposed vehicle and S3I-201–treated mice (mean ± SE; $n = 5$–7 mice per group; *t* test, $P =$ no significance).

in egg-exposed mice. Thus, the top genes, networks, and functions that we identified as differentially expressed were largely metabolic and inflammatory, which likely represents cellular activity primarily within the regions of granulomatous inflammation. Consequently, we searched for candidate modulated pathways that were likely to be involved specifically in the vascular remodeling phenotype, confirmed the location of altered activity by immunostaining, and confirmed the role of the IL-6–STAT3–NFATc2 pathway by direct intervention.

Transcriptome analysis suggested an up-regulation of the IL-6–STAT3–NFATc2 pathway, which was confirmed to be up-regulated in both peri-egg granulomas and remodeled vessels by protein-level assessments. Up-regulation of the same pathway is seen in other PH disease models, including chronic hypoxia in both the mouse and rat and in human IPAH (20–22). The ablation of IL-6 was found to be protective in the chronic hypoxia model (28). In contrast, we found that the genetic or pharmacological lack of IL-6 signaling (at the level of either IL-6 or STAT3, respectively) promoted the remodeling of the endothelial layer after *S. mansoni* exposure. Media remodeling was decreased in IL-$6^{-/-}$ mice, and increased in mice treated with a STAT3 inhibitor. The medial protection observed in IL-$6^{-/-}$ mice treated with either hypoxia or *Schistosoma* may indicate common pathogenic mechanisms. The different phenotype with STAT3 inhibition may be a result of alternative IL-6 signaling pathways (e.g., through phosphoinositide 3-kinase (PI3K)/AKR mice thymoma (Akt)) (29) or dose-specific or compartment-specific effects of the pharmacological inhibitor. In contrast, the deleterious effects we observed on the intimal layer induced by the IL-6 signaling blockade may involve the more robust Th2 inflammation triggered by *S. mansoni* exposure. Although macrophages, when alternatively activated by hypoxia, participate in hypoxia-induced PH (7), the schistosomiasis PH model shows more explicit Th2 inflammation in comparison with hypoxia.

We identified a colocalization of IL-6 with the macrophage marker Mac3, suggesting that macrophages (likely to be alternatively activated after *S. mansoni* exposure) are a key source of IL-6 in our disease model. IL-6 is known to be secreted by macrophages and other cell types, including mast cells (30, 31). Our recent data indicate that macrophages are also the source of TGF-β, which contributes to schistosomiasis-induced PH (Graham and colleagues, unpublished findings). The macrophage population (which may be heterogenous) may be secreting a spectrum of factors that are pathologic in this disease.

Transcriptome analysis also suggested the up-regulation of two other pathways, Ang–Tie2–survivin and NF-κB–Chi3l1. Tie2 haploinsufficiency is able to cause spontaneous PH in the mouse, and when coupled with IL-6 exposure, can further exacerbate the phenotype (32). Human PAH demonstrates

increased levels of vascular survivin, an antiapoptotic factor negatively regulated by Tie2 (33). Chi3l1 has been implicated in Th2-induced airway muscle remodeling, and thus would be an intriguing pathway to investigate for vascular remodeling (34). The protein levels of both Ang2 and Survivin were up-regulated, with the increased survivin primarily localized to the adventitia. However, protein levels of phospho-p65 and total p65 were not significantly altered, and Chi3l1, although up-regulated, localized primarily to the respiratory epithelium and peri-egg granulomas of *S. mansoni* egg–exposed mice, and not to the remodeled vessels. Pulmonary vascular survivin was increased in patients who died of this disease.

Overall, we found that whole-lung transcriptome analysis identified the IL-6–STAT3–NFATc2 pathway as up-regulated around and within remodeled vessels in *S. mansoni* egg–exposed mice, comparable to the pathology present in human tissue from patients with this condition. In contrast to the chronic hypoxia-PH model, in which IL-6 appears to be pathogenic, our data indicate that IL-6 signaling may instead be protective, particularly in the endothelial compartment, in *Schistosoma*-induced PH.

Author disclosures are available with the text of this article at www.atsjournals.org.

Acknowledgments: *S. mansoni*–infected mice were provided by Biomedical Research Institute via the National Institute of Allergy and Infectious Diseases (NIAID) Schistosomiasis Resource Center under National Institutes of Health–NIAID contract HHSN272201000005I.

References

1. Chitsulo L, Loverde P, Engels D. Schistosomiasis. *Nat Rev Microbiol* 2004;2:12–13.
2. de Cleva R, Herman P, Pugliese V, Zilberstein B, Saad WA, Rodrigues JJ, Laudanna AA. Prevalence of pulmonary hypertension in patients with hepatosplenic Mansonic schistosomiasis: prospective study. *Hepatogastroenterology* 2003;50:2028–2030.
3. Graham BB, Bandeira AP, Morrell NW, Butrous G, Tuder RM. Schistosomiasis-associated pulmonary hypertension: pulmonary vascular disease: the global perspective. *Chest* 2010;137:20S–29S.
4. Lapa M, Dias B, Jardim C, Fernandes CJ, Dourado PM, Figueiredo M, Farias A, Tsutsui J, Terra-Filho M, Humbert M, *et al.* Cardiopulmonary manifestations of hepatosplenic schistosomiasis. *Circulation* 2009;119: 1518–1523.
5. Tuder RM. Pathology of pulmonary arterial hypertension. *Semin Respir Crit Care Med* 2009;30:376–385.
6. Dorfmüller P, Perros F, Balabanian K, Humbert M. Inflammation in pulmonary arterial hypertension. *Eur Respir J* 2003;22:358–363.
7. Vergadi E, Chang MS, Lee C, Liang OD, Liu X, Fernandez-Gonzalez A, Mitsialis SA, Kourembanas S. Early macrophage recruitment and alternative activation are critical for the later development of hypoxia-induced pulmonary hypertension. *Circulation* 2011;123:1986–1995.
8. Graham BB, Mentink-Kane MM, El-Haddad H, Purnell S, Zhang L, Zaiman A, Redente EF, Riches DW, Hassoun PM, Bandeira A, *et al.* Schistosomiasis-induced experimental pulmonary hypertension: role of interleukin-13 signaling. *Am J Pathol* 2010;177:1549–1561.
9. Crosby A, Jones FM, Southwood M, Dunne DW, Morrell NW. Praziquantel prevents progression of right ventricular hypertrophy in a mouse model of schistosomiasis. *Am J Respir Crit Care Med* 2010;181:A4895.
10. Crosby A, Jones FM, Southwood M, Stewart S, Schermuly R, Butrous G, Dunne DW, Morrell NW. Pulmonary vascular remodeling correlates with lung eggs and cytokines in murine schistosomiasis. *Am J Respir Crit Care Med* 2010;181:279–288.
11. Daley E, Emson C, Guignabert C, de Waal Malefyt R, Louten J, Kurup VP, Hogaboam C, Taraseviciene-Stewart L, Voelkel NF, Rabinovitch M, *et al.* Pulmonary arterial remodeling induced by a Th2 immune response. *J Exp Med* 2008;205:361–372.
12. Cho WK, Lee CM, Kang MJ, Huang Y, Giordano FJ, Lee PJ, Trow TK, Homer RJ, Sessa WC, Elias JA, *et al.* IL-13 receptor alpha2–arginase2 pathway mediates IL-13–induced pulmonary hypertension. *Am J Physiol Lung Cell Mol Physiol* 2013;304:L112–124.
13. Graham BB, Chabon J, Kolosionek E, Edwards M, Bandeira A, Geraci M, Butrous G, Tuder R. Whole lung transcriptome analysis of a model of schistosomiasis-associated pulmonary hypertension [abstract]. *Am J Respir Crit Care Med* 2012;185:A3433.
14. Bauer MJ, Cox AJ, Evers DJ. ELANDv2 - fast gapped read mapping for illumina reads. In: Proceeding of the 18th annual conference on intelligent systems for molecular biology. La Jolla: International Society for Computational Biology; 2010. p. J04.
15. Trapnell C, Williams BA, Pertea G, Mortazavi A, Kwan G, van Baren MJ, Salzberg SL, Wold BJ, Pachter L. Transcript assembly and quantification by RNA-seq reveals unannotated transcripts and isoform switching during cell differentiation. *Nat Biotechnol* 2010;28:511–515.
16. Trapnell C, Pachter L, Salzberg SL. TopHat: discovering splice junctions with RNA-seq. *Bioinformatics* 2009;25:1105–1111.
17. Langmead B, Trapnell C, Pop M, Salzberg SL. Ultrafast and memory-efficient alignment of short DNA sequences to the human genome. *Genome Biol* 2009;10:R25.
18. Augustin HG, Koh GY, Thurston G, Alitalo K. Control of vascular morphogenesis and homeostasis through the angiopoietin–Tie system. *Nat Rev Mol Cell Biol* 2009;10:165–177.
19. Recklies AD, Ling H, White C, Bernier SM. Inflammatory cytokines induce production of Chi3l1 by articular chondrocytes. *J Biol Chem* 2005;280:41213–41221.
20. Bonnet S, Rochefort G, Sutendra G, Archer SL, Haromy A, Webster L, Hashimoto K, Bonnet SN, Michelakis ED. The nuclear factor of activated T cells in pulmonary arterial hypertension can be therapeutically targeted. *Proc Natl Acad Sci USA* 2007;104:11418–11423.
21. Courboulin A, Paulin R, Giguère NJ, Saksouk N, Perreault T, Meloche J, Paquet ER, Biardel S, Provencher S, Côté J, *et al.* Role for miR-204 in human pulmonary arterial hypertension. *J Exp Med* 2011;208: 535–548.
22. Steiner MK, Syrkina OL, Kolliputi N, Mark EJ, Hales CA, Waxman AB. Interleukin-6 overexpression induces pulmonary hypertension. *Circ Res* 2009;104:236–244.
23. Chen JW, Murphy TL, Willingham MC, Pastan I, August JT. Identification of two lysosomal membrane glycoproteins. *J Cell Biol* 1985;101:85–95.
24. de Jesus AR, Silva A, Santana LB, Magalhães A, de Jesus AA, de Almeida RP, Rêgo MA, Burattini MN, Pearce EJ, Carvalho EM. Clinical and immunologic evaluation of 31 patients with acute schistosomiasis mansoni. *J Infect Dis* 2002;185:98–105.
25. Johnson AW, Kinzenbaw DA, Modrick ML, Faraci FM. Small-molecule inhibitors of signal transducer and activator of transcription 3 protect against angiotensin II–induced vascular dysfunction and hypertension. *Hypertension* 2013;61:437–442.
26. Beane J, Vick J, Schembri F, Anderlind C, Gower A, Campbell J, Luo L, Zhang XH, Xiao J, Alekseyev YO, *et al.* Characterizing the impact of smoking and lung cancer on the airway transcriptome using RNA-seq. *Cancer Prev Res (Phila)* 2011;4:803–817.
27. Garber M, Grabherr MG, Guttman M, Trapnell C. Computational methods for transcriptome annotation and quantification using RNA-seq. *Nat Methods* 2011;8:469–477.
28. Savale L, Tu L, Rideau D, Izziki M, Maitre B, Adnot S, Eddahibi S. Impact of interleukin-6 on hypoxia-induced pulmonary hypertension and lung inflammation in mice. *Respir Res* 2009;10:6.
29. Condorelli G, Drusco A, Stassi G, Bellacosa A, Roncarati R, Iaccarino G, Russo MA, Gu Y, Dalton N, Chung C, *et al.* Akt induces enhanced myocardial contractility and cell size *in vivo* in transgenic mice. *Proc Natl Acad Sci USA* 2002;99:12333–12338.
30. Diehl S, Rincón M. The two faces of IL-6 on Th1/Th2 differentiation. *Mol Immunol* 2002;39:531–536.
31. Ganeshan K, Bryce PJ. Regulatory T cells enhance mast cell production of IL-6 via surface-bound TGF-β. *J Immunol* 2012;188:594–603.
32. Kugathasan L, Ray JB, Deng Y, Rezaei E, Dumont DJ, Stewart DJ. The angiopietin-1–Tie2 pathway prevents rather than promotes pulmonary arterial hypertension in transgenic mice. *J Exp Med* 2009;206: 2221–2234.
33. McMurtry MS, Archer SL, Altieri DC, Bonnet S, Haromy A, Harry G, Bonnet S, Puttagunta L, Michelakis ED. Gene therapy targeting survivin selectively induces pulmonary vascular apoptosis and reverses pulmonary arterial hypertension. *J Clin Invest* 2005;115:1479–1491.
34. Cunningham J, Basu K, Tavendale R, Palmer CN, Smith H, Mukhopadhyay S. The Chi3l1 rs4950928 polymorphism is associated with asthma-related hospital admissions in children and young adults. *Ann Allergy Asthma Immunol* 2011;106:381–386.